An Allosteric Pathway in Copper, Zinc Superoxide Dismutase Unravels the Molecular Mechanism of the G93A Amyotrophic Lateral Sclerosis-Linked Mutation

Souza, Paulo C. T.; Thallmair, Sebastian; Marrink, Siewert J.; Mera-Adasme, Raul

Published in:
JOURNAL OF PHYSICAL CHEMISTRY LETTERS

DOI:
10.1021/acs.jpclett.9b02868

Publication date:
2019

THE JOURNAL OF PHYSICAL CHEMISTRY Letters

Letter

Cite This: J. Phys. Chem. Lett. 2019, 10, 7740−7744

pubs.acs.org/JPCL

An Allosteric Pathway in Copper, Zinc Superoxide Dismutase Unravels the Molecular Mechanism of the G93A Amyotrophic Lateral Sclerosis-Linked Mutation

Paulo C. T. Souza,[†] Sebastian Thallmair,[†] Siewert J. Marrink,*[,†] and Raúl Mera-Adasme*[,‡]

[†]Groningen Biomolecular Sciences and Biotechnology Institute, University of Groningen, Nijenborgh 4, 9747 AG Groningen, The Netherlands

[‡]Departamento de Ciencias del Ambiente, Facultad de Química y Biología, Universidad de Santiago de Chile (USACH), Av. Libertador Bernardo O'Higgins 3363, 9170022 Estacion Central, Chile

Supporting Information

ABSTRACT: Several different mutations of the protein copper, zinc superoxide dismutase (SOD1) produce the neurodegenerative disorder amyotrophic lateral sclerosis (ALS). The molecular mechanism by which the diverse mutations converge to a similar pathology is currently unknown. The electrostatic loop (EL) of SOD1 is known to be affected in all of the studied ALS-linked mutations of SOD1. In this work, we employ a multiscale simulation approach to show that this perturbation corresponds to an increased probability of the EL detaching from its native position, exposing the metal site of the protein to water. From extensive atomistic and coarse-grained molecular dynamics (MD) simulations, we identify an allosteric pathway that explains the action of the distant G93A mutation on the EL. Finally, we employ quantum mechanics/molecular mechanics MD simulations to show that the opening of the EL decreases the Zn(II) affinity of the protein. As the loss of Zn(II) is at the center of several proposed pathogenic mechanisms in SOD1-linked ALS, the structural effect identified here not only is in agreement with the experimental data but also places the opening of the electrostatic loop as the possible main pathogenic effect for a significant number of ALS-linked SOD1 mutations.

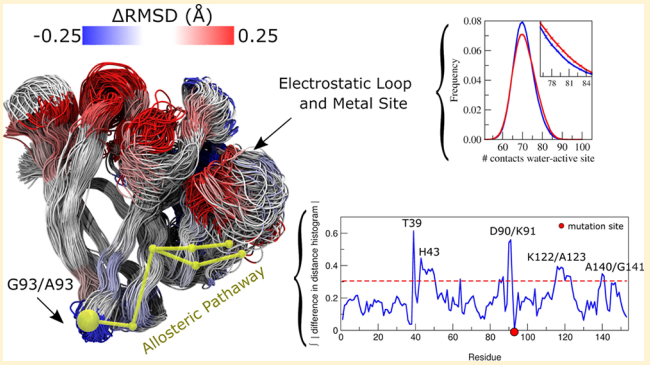

The protein copper, zinc superoxide dismutase (SOD1) catalyzes the dismutation of the superoxide radical into molecular oxygen and peroxide.[1] It protects the cell from the radical, which is naturally formed during cell respiration. Human SOD1 is a dimeric protein, which binds a Zn(II) and a Cu(I/II) ion per monomer (see Figure 1A,B).

Well more than 100 mutations, scattered along the whole sequence of SOD1, are linked to familial forms of the neurodegenerative disease amyotrophic lateral sclerosis (ALS).[2] The study of SOD1-linked cases of ALS is expected to shed light on the pathogenic mechanism of the most prevalent sporadic form of the disease. The pathogenic mechanisms of the ALS-linked mutations of SOD1 have not been elucidated in detail. The current data indicate that a gain of a pathological function is responsible for the toxicity of the mutant, rather than a loss of enzymatic activity.[3] Several hypotheses for the pathological function exist: SOD1 misfolding could interfere with cellular metabolism.[4−8] A distortion of the active site of the protein could cause aberrant redox catalysis and cellular oxidative stress.[9] Finally, a loss of metal ions, particularly Zn(II), from the SOD1 active site, could cause a harmful metal dyshomeostasis.[10−13]

A loss of Zn(II) from the active site of SOD1 appears to play a critical role in the hypotheses for SOD1 pathogenicity:[14] It destabilizes the protein's structure[15−17] and alters its active site,[18,19] and mutant SOD1 has been shown to cause Zn(II) dyshomeostasis in mice.[20] Close to the Zn(II) site of SOD1 is the electrostatic loop (EL), which is known to be destabilized in several ALS-linked mutants.[21] From a physicochemical point of view, the diversity of the pathogenic mutations, regarding both the amino acid substitution and its location in the protein structure, is intriguing. Because demetalation has been shown to be important for the misfolding process,[14] computational investigation of pathogenic mutants of SOD1 has been preferentially performed on the zinc-deficient apoenzyme,[7,8,18] confirming that ALS-linked mutations also increase the level of oligomerization. Mera-Adasme and collaborators have investigated the effect of SOD1 mutations on the metal site by means of computational chemistry.[22,23] Their focus was exclusively on mutations in the proximity of the metal site,

Received: September 28, 2019
Accepted: November 20, 2019
Published: November 20, 2019

DOI: 10.1021/acs.jpclett.9b02868
J. Phys. Chem. Lett. 2019, 10, 7740−7744

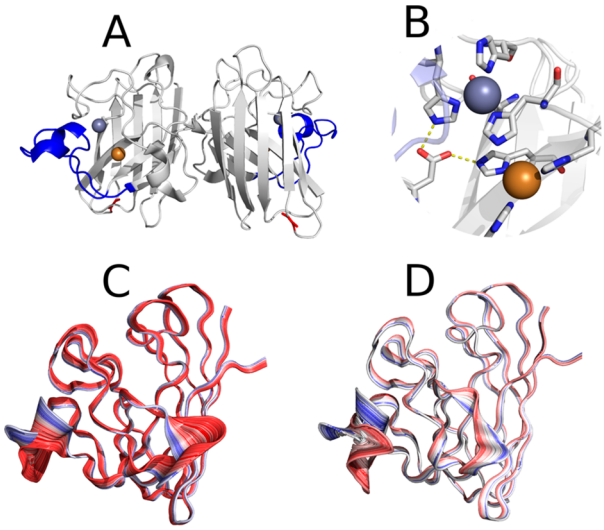

Figure 1. Atomistic structure and dynamics of SOD1. (A) Ribbon view of the crystallographic structure of dimeric SOD1.[27] The EL is colored blue; the G93 residue is shown as red sticks, and Cu(I) and Zn(II) ions are shown as orange and gray spheres, respectively. (B) Details of the metal site. Oxygen atoms are colored red, and nitrogen atoms blue. (C and D) Superimposed frames colored from blue to white to red for the first eigenvector of the covariance matrix for WT and G93A mutant MD trajectories, respectively, where the EL opening can be seen.

where altered Zn(II) binding or interactions with the EL determined the impact of the mutations. The effect of non-active site mutations of SOD1 on the metal affinity of the protein and the underlying molecular mechanisms are still unclear. To the best of our knowledge, neither aspect has been elucidated.

This work focuses on the G93A mutation of SOD1, a widely studied mutation, as the expression of its human form in mice constitutes a common animal model of ALS.[24] Because the mutation occurs away from the metal site (Figure 1, top), it must affect the metal site allosterically. While the G93A mutant is experimentally known to affect the EL and the metal site of the protein,[20,21,25] the effect is subtle, as only a methyl group is added, and the purified variant has also been shown to be metalated and catalytically active.[26] We use atomistic and coarse-grained (CG) molecular dynamics (MD) simulations of the SOD1 wild type (WT) and its G93A mutant to compare their EL loop opening. Moreover, to evaluate the impact of the EL loop opening on the metal site, we also perform hybrid quantum mechanical/molecular mechanical (QM/MM) MD simulations. The thorough statistics from the CG simulations allow us to identify for the first time the allosteric pathway from the distant G93A mutation to the metal site of SOD1.

We performed atomistic MD simulations on models for the monomer of the wild type (WT) and G93A variants of human SOD1, both derived from the high-resolution crystallographic structure for the WT enzyme.[27] Three 1 μs simulations were performed for each variant and show a stable protein fold. In one of the mutant trajectories and two of the WT ones, full opening of the EL could be observed (Figures S4 and S5). During the opening, weak interactions between one half of the loop and the rest of the protein are broken, and the detached loop adopts a distorted configuration (Figure 1C,D). The "open" half of the loop matches the amino acid sequence previously shown by H/D exchange to have enhanced hydration in ALS-linked mutants of SOD1.[21] However, the obtained atomistic simulation times are insufficient for judging whether there is an altered tendency for loop opening in G93A SOD1.

To obtain reliable statistics, we performed CG MD simulations with the Martini force field. To the best of our knowledge, this is not only the first exploration of the combined Martini 3 (open-beta version[28−30]) and Gō-like models[31] but also among the first uses of Martini for the study of a conformational transition in a protein.[28,32] A total of 480 μs of simulation time (12 × 40 μs) was obtained for each variant (WT and G93A) of SOD1. The CG simulations revealed similar EL opening events compared to the atomistic simulations, indicating that the CG model reliably reproduces the protein flexibility. Figure 2 summarizes the key findings of

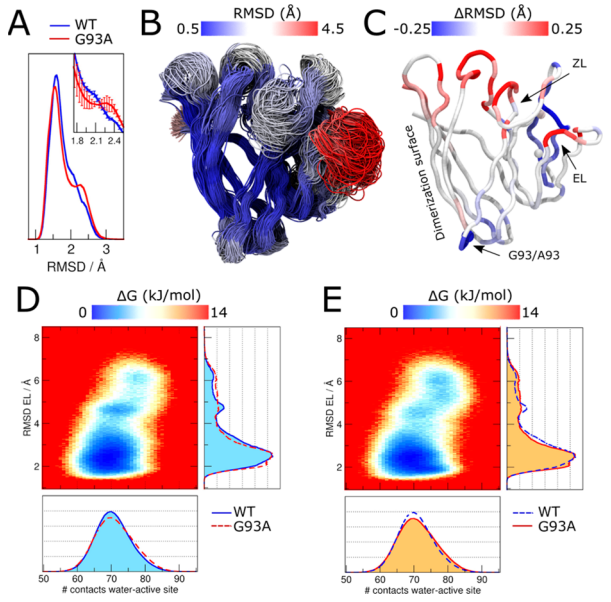

Figure 2. Comparison of the SOD1 WT and G93A mutant based on the CG Martini simulations. (A) Distribution of the average protein backbone RMSD for the WT (blue) and the G93A mutant (red) obtained from 480 μs of simulation each. The inset shows the region between 1.75 and 2.55 Å including error bars. (B) Flexibility of the protein backbone of the WT. Snapshots were taken every 1 μs; the color scale represents the backbone RMSD. (C) Change in RMSD between the WT and G93A. Blue indicates rigidification in G93A; red indicates increased flexibility. (D and E) Free energy surfaces of WT and G93A, respectively, spanned by the EL RMSD and the water−active site contacts (top left). The underlying probability distribution of the EL RMSD (top right) and the number of water−active site contacts (bottom) are also depicted. The differences in the probability distributions are small, but meaningful as shown by the error bars in Figure S6. For the sake of clarity, the error bars have been omitted.

the CG simulations. The distribution of the average protein backbone root-mean-square deviation (RMSD) depicted in Figure 2A has a similar maximum position for the WT (blue) and the G93A mutant (red). However, above an RMSD of 2.3 Å, a clear shoulder is present in the mutant that is missing in the WT. Thus, the mutation results in an increased population at a higher RMSD. Figure 2B shows that the EL exhibits the highest RMSD of ∼4.5 Å in the case of the WT, indicating that the shoulder at the high RMSD might impact the EL to a large extent. Interestingly, the vicinity of the mutation site in the G93A mutant becomes rigid compared to that of the WT (see

DOI: 10.1021/acs.jpclett.9b02868
J. Phys. Chem. Lett. 2019, 10, 7740−7744

Figure 2C). In contrast, the EL exhibits an increased flexibility in the mutant, which is in agreement with the experimentally reported increased mobility of the SOD1 EL.[21] Moreover, the increased flexibility of the Zn loop (ZL) as well as the unaffected dimerization surface are in agreement with observations from H/D exchange experiments.[25]

The G93A mutation has been shown to impair the Zn metabolism in the cell and to destabilize the metal site.[6,20,25] We had previously proposed an increased level of hydration of the metal site via EL opening, resulting in a decreased affinity of SOD1 for Zn(II), as a pathogenic mechanism for ALS-linked SOD1 mutants.[22,33] We analyzed the number of contacts between the active site of SOD1 and CG water beads. The G93A mutant shows more water−active site contacts than the WT (bottom panels in Figure 2D,E). Note that one CG water bead represents four water molecules. Thus, 1.5 CG water beads are sufficient to form a hexaaqua complex with the Cu(I/II) or Zn(II) ions. To resolve the connection between the water−active site contacts and the RMSD of the EL, we calculated the corresponding two-dimensional free energy surface for the WT (Figure 2D) and the G93A mutant (Figure 2E). In both cases, the global minimum is located at a low RMSD (∼2.5 Å) and ∼70 water−active site contacts. A closer look at the tail of the minimum at a higher RMSD reveals that the G93A mutant exhibits a wider and slightly deeper minimum at an RMSD of ∼6 Å and ∼80 water−active site contacts. Overall, our CG simulations show a stronger tendency for EL opening in the G93A mutant, in agreement with experimental observations, together with a higher level of hydration of the active site.

To determine whether the increased level of hydration of the metal site has an effect on the binding energy of Zn(II), implicated in proposed mechanisms for SOD1 pathogenic function, we performed QM/MM MD simulations starting from structures taken from the atomistic trajectories (see Figure 3A,B). The QM subsystem, treated at the composite HF-3c level of theory, contained 590 atoms, in line with what we previously showed to be adequate[34] (see the Supporting Information). Four simulations of 4 ps each were performed: with the EL in open and closed configurations and, for each of them, with and without Zn(II) bound to the protein. Subtraction of the potential energy averages for the trajectories can be assimilated to the difference in $\Delta\Delta H$ of Zn(II) binding between the protein in open and closed EL conformations. The closed EL conformation has a more favorable ΔH of Zn(II) binding by −99 kJ/mol. A frequency-based estimation for the $\Delta\Delta S$ for the process, employing the full protein plus the water molecules within ∼10 Å of the metal site (see the Supporting Information), gave a $-T\Delta\Delta S$ value of 15 kJ/mol, close to an order of magnitude lower than the calculated $\Delta\Delta H$.

To unravel the pathway transmitting the subtle mutation G93A toward the EL, we analyzed the distance distributions between all pairwise residue combinations in the CG trajectories (as described in Figures S3 and S8A,B). The integrated absolute differences between the distance distributions of the WT and the G93A mutant are depicted in Figure 3C. The largest changes are observed between the region of residues 90−95 (around the mutation site) and all other residues. In Figure 3D, the residues of the SOD1 monomer for which the integrated absolute difference between the distance distributions of mutation site 93 and all other residues is larger than 0.3 are colored red. Besides the vicinity of the mutation site, several residues connecting the mutation site with the joint for the EL opening (residues 122 and 141) exhibit significant differences in the distance distributions (see Figure S8C,D).

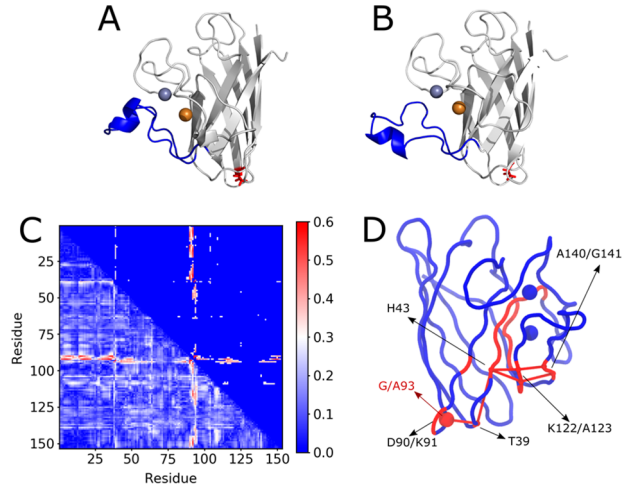

Figure 3. (A and B) QM/MM-optimized structures for the G93A mutant in the closed and open EL conformations, respectively. The EL is colored blue; the G93 residue is shown as red sticks, and Cu(I) and Zn(II) ions are shown as orange and gray spheres, respectively. (C) Matrix representation of the integrated absolute difference in the distance distributions between all backbone beads. The bottom left triangle represents the full data set. In the top right triangle, only values of >0.3 are depicted; all other values are colored blue. (D) Residues exhibiting an integrated absolute difference between the distributions of the distance of the respective residue and the mutation site of WT and G93A of >0.3 are colored red. The red bonds between the backbone chain indicate transfer pathways based on the Gō-like model.

A closer look at the atomistic structure reveals a network comprising hydrogen and peptide bonds that are responsible for the mechanical communication of G93 with the EL. The backbone of L38 is closely packed with G93 in the WT structure and directly linked to the first residue in the network, T39. The packing is altered in the mutant by a steric clash between C_β of A93 and the backbone oxygen of L38. This clash can also be observed in our atomistic simulations resulting in a change in the G/A93($C_{\beta3}$)−L38(O) distance distribution (see Figures S9 and S10). The identified network promotes this altered distance via three hydrogen and two peptide bonds toward the joint of the EL. Namely, residues T39, H43, K122, A123, A140, and G141 are involved in the network and all exhibit significant changes in their distributions (Figure S8). The allosteric pathway thus identified is comprised mainly of backbone-mediated interactions, which explains its lack of susceptibility to ALS-causing mutations, as previously discussed.[22] The exception is the H43 residue, which participates in the interactions with its side chain and is the target of at least one known ALS-causing mutation.[35]

In summary, our multiscale simulation study provides a molecular mechanism for the pathogenic effect of the widely studied G93A mutation of SOD1. Our results directly link the G93A mutation to a Zn(II) site destabilization via an increased level of electrostatic loop opening. It arises from a steric clash between G93 and L38 in the mutant. We identified a network connecting G93 with the main point of EL opening, which is responsible for transmitting the steric clash to the EL. In a more general view, our results back the general involvement of the EL in SOD1-linked ALS pathogenesis by providing

DOI: 10.1021/acs.jpclett.9b02868
J. Phys. Chem. Lett. 2019, 10, 7740−7744

molecular level insights into EL destabilization. Moreover, the results also mark a milestone in the combined use of the Martini 3 force field and Gō-like models to study long-range structural communication and allosteric changes caused by single-point mutations.

COMPUTATIONAL METHODS

All MD simulations were performed with the MD package GROMACS (version 2018).[36,37] Atomistic simulations were realized with the AMBER99SB-ILDN force field for the protein,[38,39] while metal parameters were obtained in a previous work.[40] The open-beta version of the Martini 3 force field[28,30] in combination with a Gō-like model[31] was used for the CG MD simulations. The beta release of Martini 3 is available online at the webpage of Marrink's group.[29] QM/MM calculations were performed with the program packages pDynamo,[41] ORCA 4.0,[42] Turbomole version 7.3,[43,44] and xtb.[45] The HF-3c composite method and GFN0-xTB semiempirical method from Grimme[46,47] were employed for the QM part of the system, while the AMBER-ILDN force field[38,39] was employed for the MM subsystem. Further details are given in the Supporting Information.

ASSOCIATED CONTENT

Supporting Information

The Supporting Information is available free of charge at https://pubs.acs.org/doi/10.1021/acs.jpclett.9b02868.

Computational details and parameters of atomistic MD simulations, QM/MM simulations, and CG MD simulations; and additional analysis, including the flexibility of the EL loop in atomistic simulations, RMSD and hydration analysis of the CG simulations, significance of the QM/MM energy values, comparison of backbone bead distributions of the CG simulations, and impact of the mutation on the 93C−38O distance (PDF)

AUTHOR INFORMATION

Corresponding Authors

*E-mail: s.j.marrink@rug.nl.

*E-mail: raul.mera@usach.cl.

ORCID

Paulo C. T. Souza: 0000-0003-0660-1301

Sebastian Thallmair: 0000-0002-3396-5840

Siewert J. Marrink: 0000-0001-8423-5277

Raúl Mera-Adasme: 0000-0003-0345-6217

Author Contributions

All authors designed the research. P.C.T.S., S.T., and R.M.-A. performed the simulations. All authors analyzed the data. The manuscript was written by P.C.T.S., S.T., and R.M.-A. with suggestions from S.J.M. All authors have given approval to the final version of the manuscript.

Notes

The authors declare no competing financial interest.

ACKNOWLEDGMENTS

R.M.-A. thanks CONICYT-Chile for support under FONDECYT N° 11160032. S.T. thanks the European Commission for support via a Marie Skłodowska-Curie Actions Individual Fellowship (MicroMod-PSII, Grant Agreement 748895). P.C.T.S., S.T., and S.J.M. acknowledge the National Computing Facilities Foundation (NCF) of The Netherlands Organization for Scientific Research (NWO) for providing computing time.

REFERENCES

(1) Hart, P. J.; Balbirnie, M. M.; Ogihara, N. L.; Nersissian, A. M.; Weiss, M. S.; Valentine, J. S.; Eisenberg, D. A Structure-Based Mechanism for Copper−Zinc Superoxide Dismutase. *Biochemistry* **1999**, *38* (7), 2167−2178.

(2) Wroe, R.; Wai-Ling Butler, A.; Andersen, P. M.; Powell, J. F.; Al-Chalabi, A. ALSOD: The Amyotrophic Lateral Sclerosis Online Database. *Amyotrophic Lateral Scler.* **2008**, *9* (4), 249−250.

(3) Valentine, J. S.; Hart, P. J. Misfolded CuZnSOD and Amyotrophic Lateral Sclerosis. *Proc. Natl. Acad. Sci. U. S. A.* **2003**, *100* (7), 3617−3622.

(4) Ido, A.; Fukuyama, H.; Urushitani, M. Protein Misdirection inside and Outside Motor Neurons in Amyotrophic Lateral Sclerosis (ALS): A Possible Clue for Therapeutic Strategies. *Int. J. Mol. Sci.* **2011**, *12* (10), 6980−7003.

(5) Perry, J. J. P.; Shin, D. S.; Getzoff, E. D.; Tainer, J. A. The Structural Biochemistry of the Superoxide Dismutases. *Biochim. Biophys. Acta, Proteins Proteomics* **2010**, *1804* (2), 245−262.

(6) Kim, J. M.; Billington, E.; Reyes, A.; Notarianni, T.; Sage, J.; Agbas, E.; Taylor, M.; Monast, I.; Stanford, J. A.; Agbas, A. Impaired Cu-Zn Superoxide Dismutase (SOD1) and Calcineurin (Cn) Interaction in ALS: A Presumed Consequence for TDP-43 and Zinc Aggregation in Tg SOD1G93A Rodent Spinal Cord Tissue. *Neurochem. Res.* **2019**, *44* (1), 228−233.

(7) Khare, S. D.; Dokholyan, N. V. Common Dynamical Signatures of Familial Amyotrophic Lateral Sclerosis-Associated Structurally Diverse Cu, Zn Superoxide Dismutase Mutants. *Proc. Natl. Acad. Sci. U. S. A.* **2006**, *103* (9), 3147−3152.

(8) Proctor, E. A.; Fee, L.; Tao, Y.; Redler, R. L.; Fay, J. M.; Zhang, Y.; Lv, Z.; Mercer, I. P.; Deshmukh, M.; Lyubchenko, Y. L.; et al. Nonnative SOD1 Trimer Is Toxic to Motor Neurons in a Model of Amyotrophic Lateral Sclerosis. *Proc. Natl. Acad. Sci. U. S. A.* **2016**, *113* (3), 614−619.

(9) Crow, J. P.; Sampson, J. B.; Zhuang, Y.; Thompson, J. A.; Beckman, J. S. Decreased Zinc Affinity of Amyotrophic Lateral Sclerosis-Associated Superoxide Dismutase Mutants Leads to Enhanced Catalysis of Tyrosine Nitration by Peroxynitrite. *J. Neurochem.* **1997**, *69* (5), 1936−1944.

(10) Smith, A. P.; Lee, N. M. Role of Zinc in ALS. *Amyotrophic Lateral Scler.* **2007**, *8* (3), 131−143.

(11) Nagano, S.; Satoh, M.; Sumi, H.; Fujimura, H.; Tohyama, C.; Yanagihara, T.; Sakoda, S. Reduction of Metallothioneins Promotes the Disease Expression of Familial Amyotrophic Lateral Sclerosis Mice in a Dose-Dependent Manner. *Eur. J. Neurosci.* **2001**, *13* (7), 1363−1370.

(12) Hashimoto, K.; Hayashi, Y.; Watabe, K.; Inuzuka, T.; Hozumi, I. Metallothionein-III Prevents Neuronal Death and Prolongs Life Span in Amyotrophic Lateral Sclerosis Model Mice. *Neuroscience* **2011**, *189*, 293−298.

(13) Kaneko, M.; Noguchi, T.; Ikegami, S.; Sakurai, T.; Kakita, A.; Toyoshima, Y.; Kambe, T.; Yamada, M.; Inden, M.; Hara, H.; et al. Zinc Transporters ZnT3 and ZnT6 Are Downregulated in the Spinal Cords of Patients with Sporadic Amyotrophic Lateral Sclerosis. *J. Neurosci. Res.* **2015**, *93* (2), 370−379.

(14) Sirangelo, I.; Iannuzzi, C. The Role of Metal Binding in the Amyotrophic Lateral Sclerosis-Related Aggregation of Copper-Zinc Superoxide Dismutase. *Molecules* **2017**, *22* (9), E1429.

(15) Kayatekin, C.; Zitzewitz, J. A.; Matthews, C. R. Zinc Binding Modulates the Entire Folding Free Energy Surface of Human Cu,Zn Superoxide Dismutase. *J. Mol. Biol.* **2008**, *384* (2), 540−555.

(16) Roberts, B. R.; Tainer, J. A.; Getzoff, E. D.; Malencik, D. A.; Anderson, S. R.; Bomben, V. C.; Meyers, K. R.; Karplus, P. A.; Beckman, J. S. Structural Characterization of Zinc-Deficient Human

DOI: 10.1021/acs.jpclett.9b02868
J. Phys. Chem. Lett. 2019, 10, 7740−7744

Superoxide Dismutase and Implications for ALS. *J. Mol. Biol.* **2007**, *373* (4), 877−890.
(17) Ding, F.; Dokholyan, N. V. Dynamical Roles of Metal Ions and the Disulfide Bond in Cu, Zn Superoxide Dismutase Folding and Aggregation. *Proc. Natl. Acad. Sci. U. S. A.* **2008**, *105* (50), 19696−19701.
(18) Nedd, S.; Redler, R. L.; Proctor, E. A.; Dokholyan, N. V.; Alexandrova, A. N. Cu,Zn-Superoxide Dismutase without Zn Is Folded but Catalytically Inactive. *J. Mol. Biol.* **2014**, *426* (24), 4112−4124.
(19) Trumbull, K. A.; Beckman, J. S. A Role for Copper in the Toxicity of Zinc-Deficient Superoxide Dismutase to Motor Neurons in Amyotrophic Lateral Sclerosis. *Antioxid. Redox Signaling* **2009**, *11* (7), 1627−1639.
(20) Kim, J.; Kim, T.-Y.; Hwang, J. J.; Lee, J.-Y.; Shin, J.-H.; Gwag, B. J.; Koh, J.-Y. Accumulation of Labile Zinc in Neurons and Astrocytes in the Spinal Cords of G93A SOD-1 Transgenic Mice. *Neurobiol. Dis.* **2009**, *34* (2), 221−229.
(21) Molnar, K. S.; Karabacak, N. M.; Johnson, J. L.; Wang, Q.; Tiwari, A.; Hayward, L. J.; Coales, S. J.; Hamuro, Y.; Agar, J. N. A Common Property of Amyotrophic Lateral Sclerosis-Associated Variants: Destabilization of the Copper/zinc Superoxide Dismutase Electrostatic Loop. *J. Biol. Chem.* **2009**, *284* (45), 30965−30973.
(22) Mera-Adasme, R.; Erdmann, H.; Bereźniak, T.; Ochsenfeld, C. Destabilization of the Metal Site as a Hub for the Pathogenic Mechanism of Five ALS-Linked Mutants of Copper, Zinc Superoxide Dismutase. *Metallomics* **2016**, *8* (10), 1141−1150.
(23) Mera-Adasme, R.; Mendizábal, F.; Gonzalez, M.; Miranda-Rojas, S.; Olea-Azar, C.; Sundholm, D. Computational Studies of the Metal-Binding Site of the Wild-Type and the H46R Mutant of the Copper, Zinc Superoxide Dismutase. *Inorg. Chem.* **2012**, *51* (10), 5561−5568.
(24) Kim, R. B.; Irvin, C. W.; Tilva, K. R.; Mitchell, C. S. State of the Field: An Informatics-Based Systematic Review of the SOD1-G93A Amyotrophic Lateral Sclerosis Transgenic Mouse Model. *Amyotrophic Lateral Scler. Frontotemporal Degener.* **2016**, *17* (1−2), 1−14.
(25) Museth, A. K.; Brorsson, A.-C.; Lundqvist, M.; Tibell, L. A. E.; Jonsson, B.-H. The ALS-Associated Mutation G93A in Human Copper-Zinc Superoxide Dismutase Selectively Destabilizes the Remote Metal Binding Region. *Biochemistry* **2009**, *48* (37), 8817−8829.
(26) Hayward, L. J.; Rodriguez, J. A.; Kim, J. W.; Tiwari, A.; Goto, J. J.; Cabelli, D. E.; Valentine, J. S.; Brown, R. H., Jr Decreased Metallation and Activity in Subsets of Mutant Superoxide Dismutases Associated with Familial Amyotrophic Lateral Sclerosis. *J. Biol. Chem.* **2002**, *277* (18), 15923−15931.
(27) Strange, R. W.; Antonyuk, S. V.; Hough, M. A.; Doucette, P. A.; Valentine, J. S.; Hasnain, S. S. Variable Metallation of Human Superoxide Dismutase: Atomic Resolution Crystal Structures of Cu-Zn, Zn-Zn and as-Isolated Wild-Type Enzymes. *J. Mol. Biol.* **2006**, *356* (5), 1152−1162.
(28) Marrink, S. J.; Tieleman, D. P. Perspective on the Martini Model. *Chem. Soc. Rev.* **2013**, *42* (16), 6801−6822.
(29) Martini 3 open-beta version. www.cgmartini.nl/index.php/force-field-parameters/particle-definitions.
(30) Alessandri, R.; Souza, P. C. T.; Thallmair, S.; Melo, M. N.; de Vries, A. H.; Marrink, S. J. Pitfalls of the Martini Model. *J. Chem. Theory Comput.* **2019**, *15*, 5448.
(31) Poma, A. B.; Cieplak, M.; Theodorakis, P. E. Combining the MARTINI and Structure-Based Coarse-Grained Approaches for the Molecular Dynamics Studies of Conformational Transitions in Proteins. *J. Chem. Theory Comput.* **2017**, *13* (3), 1366−1374.
(32) Kmiecik, S.; Gront, D.; Kolinski, M.; Wieteska, L.; Dawid, A. E.; Kolinski, A. Coarse-Grained Protein Models and Their Applications. *Chem. Rev.* **2016**, *116* (14), 7898−7936.
(33) Mera-Adasme, R.; Suomivuori, C.-M.; Fierro, A.; Pesonen, J.; Sundholm, D. The Role of Solvent Exclusion in the Interaction between D124 and the Metal Site in SOD1: Implications for ALS. *JBIC, J. Biol. Inorg. Chem.* **2013**, *18* (8), 931−938.
(34) Mera-Adasme, R.; Domínguez, M.; Denis-Alpizar, O. A Benchmark for the Size of the QM System Required for Accurate Hybrid QM/MM Calculations on the Metal Site of the Protein Copper, Zinc Superoxide Dismutase. *J. Mol. Model.* **2019**, *25* (6), 176.
(35) Muneeswaran, G.; Kartheeswaran, S.; Muthukumar, K.; Dharmaraj, C. D.; Karunakaran, C. Comparative Structural and Conformational Studies on H43R and W32F Mutants of Copper-Zinc Superoxide Dismutase by Molecular Dynamics Simulation. *Biophys. Chem.* **2014**, *185*, 70−78.
(36) Abraham, M. J.; Murtola, T.; Schulz, R.; Páll, S.; Smith, J. C.; Hess, B.; Lindahl, E. GROMACS: High Performance Molecular Simulations through Multi-Level Parallelism from Laptops to Supercomputers. *SoftwareX* **2015**, *1−2*, 19−25.
(37) Pronk, S.; Páll, S.; Schulz, R.; Larsson, P.; Bjelkmar, P.; Apostolov, R.; Shirts, M. R.; Smith, J. C.; Kasson, P. M.; van der Spoel, D.; et al. GROMACS 4.5: A High-Throughput and Highly Parallel Open Source Molecular Simulation Toolkit. *Bioinformatics* **2013**, *29* (7), 845−854.
(38) Hornak, V.; Abel, R.; Okur, A.; Strockbine, B.; Roitberg, A.; Simmerling, C. Comparison of Multiple Amber Force Fields and Development of Improved Protein Backbone Parameters. *Proteins: Struct., Funct., Genet.* **2006**, *65* (3), 712−725.
(39) Lindorff-Larsen, K.; Piana, S.; Palmo, K.; Maragakis, P.; Klepeis, J. L.; Dror, R. O.; Shaw, D. E. Improved Side-Chain Torsion Potentials for the Amber ff99SB Protein Force Field. *Proteins: Struct., Funct., Genet.* **2010**, *78* (8), 1950−1958.
(40) Mera-Adasme, R.; Sadeghian, K.; Sundholm, D.; Ochsenfeld, C. Effect of Including Torsional Parameters for Histidine−Metal Interactions in Classical Force Fields for Metalloproteins. *J. Phys. Chem. B* **2014**, *118*, 13106−13111.
(41) Field, M. J. The pDynamo Program for Molecular Simulations Using Hybrid Quantum Chemical and Molecular Mechanical Potentials. *J. Chem. Theory Comput.* **2008**, *4* (7), 1151−1161.
(42) Neese, F. Software Update: The ORCA Program System, Version 4.0. *WIREs Comput. Mol. Sci.* **2018**, *8* (1), No. e1327.
(43) Ahlrichs, R.; Bär, M.; Häser, M.; Horn, H.; Kölmel, C. Electronic Structure Calculations on Workstation Computers: The Program System Turbomole. *Chem. Phys. Lett.* **1989**, *162* (3), 165−169.
(44) Furche, F.; Ahlrichs, R.; Hättig, C.; Klopper, W.; Sierka, M.; Weigend, F. Turbomole. *Wiley Interdiscip. Rev.: Comput. Mol. Sci.* **2014**, *4* (2), 91−100.
(45) *Xtb*. https://github.com/grimme-lab/xtb (accessed November 19, 2019).
(46) Sure, R.; Grimme, S. Corrected Small Basis Set Hartree-Fock Method for Large Systems. *J. Comput. Chem.* **2013**, *34* (19), 1672−1685.
(47) Pracht, P.; Caldeweyher, E.; Ehlert, S.; Grimme, S. A Robust Non-Self-Consistent Tight-Binding Quantum Chemistry Method for Large Molecules. *ChemRxiv* 2019.

DOI: 10.1021/acs.jpclett.9b02868
J. Phys. Chem. Lett. 2019, 10, 7740−7744